Model Calculations of Solar Spectral Irradiance in the 3.7-μm Band for Earth Remote Sensing Applications

STEVEN PLATNICK

Laboratory for Atmospheres, NASA Goddard Space Flight Center, Greenbelt, Maryland

JUAN M. FONTENLA

Laboratory for Atmospheric and Space Physics, University of Colorado, Boulder, Colorado

(Manuscript received 1 September 2006, in final form 1 February 2007)

ABSTRACT

Since the launch of the first Advanced Very High Resolution Radiometer (AVHRR) instrument aboard the Television and Infrared Observational Satellite (TIROS-N), measurements in the 3.7-μm atmospheric window have been exploited for use in cloud detection and screening, cloud thermodynamic phase and surface snow/ice discrimination, and quantitative cloud particle size retrievals. The utility of the band has led to the incorporation of similar channels on a number of existing satellite imagers and future operational imagers. Daytime observations in the band include both reflected solar and thermal emission energy. Since 3.7-μm channels are calibrated to a radiance scale (via onboard blackbodies), knowledge of the top-of-atmosphere solar irradiance in the spectral region is required to infer reflectance. Despite the ubiquity of 3.7-μm channels, absolute solar spectral irradiance data come from either a single measurement campaign (Thekaekara et al.) or synthetic spectra. In the current study, the historical 3.7-μm band spectral irradiance datasets are compared with the recent semiempirical solar model of the quiet sun by Fontenla et al. The model has expected uncertainties of about 2% in the 3.7-μm spectral region. The channel-averaged spectral irradiances using the observations reported by Thekaekara et al. are found to be 3.2%–4.1% greater than those derived from the Fontenla et al. model for Moderate Resolution Imaging Spectroradiometer (MODIS) and AVHRR instrument bandpasses; the Kurucz spectrum, as included in the Moderate Spectral Resolution Atmospheric Transmittance (MODTRAN4) distribution, gives channel-averaged irradiances 1.2%–1.5% smaller than the Fontenla model. For the MODIS instrument, these solar irradiance uncertainties result in cloud microphysical retrieval uncertainties that are comparable to other fundamental reflectance error sources.

1. Introduction

The 3.7-μm atmospheric window was first used in satellite earth remote sensing with the 1978 launch of the original four-channel Advanced Very High Resolution Radiometer (AVHRR) instrument aboard the Television and Infrared Observational Satellite (TIROS-N) polar orbiter. AVHRR has retained this spectral capability up to the present (currently through the *National Oceanic and Atmospheric Administration (NOAA)-18* polar platform, though post-*NOAA-15* platforms carry the AVHRR/3 version of the instrument, which has a single data channel shared by both 3.7- and 1.6-μm spectral channels). The main objective in originally flying the channel was reported to be for cloud screening of sea surface temperature observations (Schwalb 1978). Measurements in this window are now routinely used for cloud detection and screening (Saunders and Kriebel 1988; Ackerman et al. 1998; Heidinger et al. 2002), fire detection (Kaufman et al. 1990; Prins and Menzel 1992; Justice et al. 2002), cloud phase and surface snow/ice discrimination (Pavolonis et al. 2005), and quantitative cloud microphysical retrievals (Arking and Childs 1985; Platnick and Twomey 1994; Han et al. 1994; Minnis et al. 1995; Platnick et al. 2003). The usefulness of the band for cloud observations essentially derives from the significant dependence of single scattering albedo on cloud thermodynamic phase and particle size (absorption increases for

Corresponding author address: S. Platnick, Laboratory for Atmospheres, NASA Goddard Space Flight Center, Greenbelt, MD 20771.
E-mail: steven.platnick@nasa.gov

DOI: 10.1175/2007JAMC1571.1

the ice phase and with particle size) and differences in single scattering albedo (and thereby cloud emissivity) when compared with window IR channels. Smaller land surface emissivity relative to window bands also provides contrast. Qualitative overviews of 3.7-μm imagery from AVHRR and its uses for clouds and sea ice discrimination can be found in Scorer (1986, 1989).

The usefulness of the spectral band has led to the incorporation of a 3.7-μm channel on a number of low-earth-orbit imagers over the last decade. Examples include the Along-Track Scanning Radiometer (ATSR) on board the *European Remote Sensing Satellite-1* (*ERS-1*) and *-2* and the *Environmental Satellite* (*ENVISAT*), the Visible Infrared Scanner (VIRS) on the Tropical Rainfall Measuring Mission (TRMM) spacecraft (Barnes et al. 2000), the Moderate Resolution Imaging Spectroradiometer (MODIS) on the *Terra* and *Aqua* spacecrafts (Barnes et al. 1998), and the Global Imager (GLI) on *Midori-II* [*Advanced Earth Observing Satellite-II* (*ADEOS-II*); Nakajima et al. 1998]. On geosynchronous platforms, 3.9-μm channels are available on the new Geostationary Operational Environmental Satellite (GOES) Imager and the Meteosat Second-Generation (MSG) Spinning Enhanced Visible and Infrared Imager (SEVIRI; Aminou 2002). Future operational imagers will continue to fly similar channels for weather and climate applications, including the Visible–Infrared Imager–Radiometer Suite (VIIRS) on the National Polar-orbiting Operational Environmental Satellite System (NPOESS) and the National Aeronautics and Space Administration (NASA) NPOESS Preparatory Project (NPP; Lee et al. 2006), AVHRR/3 on the European Space Agency MetOp platforms, and the GOES-R Advanced Baseline Imager (ABI; Schmit et al. 2005). Similar channels have also been included on aircraft imagers (e.g., the MODIS Airborne Simulator flown on NASA's high-altitude ER-2 aircraft; King et al. 1996).

Daytime quantitative use of the 3.7-μm band for cloud microphysical retrievals must account for contributions from both reflected solar and thermal emission energy. The observed cloud bidirectional reflectance and emissivity, and not the measured radiance itself, are the fundamental quantities relevant for cloud microphysical retrievals. In this paper, we examine the fundamental uncertainty in the observed 3.7-μm solar reflectance that corresponds to uncertainty in the knowledge of the solar irradiance in this spectral region. The partitioning between solar and emissive radiance in practical cloud retrieval algorithms is not discussed here.

While many modern imagers have onboard solar diffusers to provide a direct reflectance calibration scale for solar spectral channels (e.g., MODIS), these calibration systems do not extend into the 3.7-μm region. A 3.7-μm channel is calibrated to a radiance scale (via onboard blackbodies), and knowledge of the top-of-atmosphere (TOA) solar irradiance across the channel's spectral bandpass is required to infer reflectance. The observed bidirectional reflectance of an earth–atmosphere scene is

$$R = \frac{\pi I}{\mu_0 F_0}, \tag{1}$$

where μ_0 is the cosine of the solar zenith angle, I is the satellite-measured radiance for the viewing geometry, and F_0 is the TOA solar irradiance. All radiative quantities in Eq. (1) are averages over the spectral bandpass of the instrument, that is,

$$F_0 = \frac{\int_{\Delta\lambda} F_0(\lambda)\Phi(\lambda)\,d\lambda}{\int_{\Delta\lambda} \Phi(\lambda)\,d\lambda},$$

$$I = \frac{\int_{\Delta\lambda} I(\lambda)\Phi(\lambda)\,d\lambda}{\int_{\Delta\lambda} \Phi(\lambda)\,d\lambda}, \quad \text{and}$$

$$R = \frac{\int_{\Delta\lambda} R(\lambda)F_0(\lambda)\Phi(\lambda)\,d\lambda}{\int_{\Delta\lambda} F_0(\lambda)\Phi(\lambda)\,d\lambda}, \tag{2}$$

where $\Phi(\lambda)$ is the instrument channel spectral response function. The relative uncertainty in reflectance because of uncertainty in the averaged irradiance over the channel can be written as

$$\frac{R_2 - R_1}{R_1} = -\frac{F_{02} - F_{01}}{F_{02}} \quad \text{and}$$
$$\frac{\Delta R}{R} \approx -\frac{\Delta F_0}{F_0}, \tag{3}$$

with F_{01} and F_{02} representing calculations from two different spectral irradiance datasets. Note the different denominator indexes in the exact expression. As an example, an overestimation in the band-averaged solar irradiance results in an underestimation of reflectance.

Despite the widespread use of 3.7-μm satellite and aircraft measurements, only a single set of observations of absolute TOA spectral irradiance from the entire solar disk has been reported in this spectral region (Thekaekara et al. 1969; Thekaekara 1974). Further, the measurements are at a relatively poor spectral resolution. Here we give an overview of the historical observational data and common synthetic datasets of spectral irradiance in the 3.7-μm band and compare these data with the new semiempirical quiet-sun model from Fontenla et al. (2006). The model's solar atmospheric parameters are adjusted to match available satellite solar spectral irradiance observations; the model explicitly includes the effect of solar activity (both the distribution and radiative effects of sunspots, plages and networks). Model irradiances in the 3.7-μm spectral region are expected to have uncertainties of about 2%; deviations from quiet-sun values are found to be less than 0.5%.

While a recent study by Trishchenko (2006) examined differences in AVHRR and GOES imager 3.7-μm band-reflected radiance and brightness temperature calculations using four solar irradiance datasets (compiled observational as well as synthetic), our current study includes a critical discussion of the original observational data as well as the new Fontenla et al. (2006) models, with an emphasis on cloud retrieval applications using the MODIS sensor.

Section 2 gives an overview of the existing 3.7-μm band absolute spectral irradiance datasets, in particular, those that have typically been used to convert radiance measurements to solar reflectances for quantitative cloud microphysical retrievals. Section 3 summarizes the Fontenla et al. (2006) set of models and compares the quiet-sun spectral irradiance with the historic datasets. The resulting differences in the band-averaged solar irradiance for 10 AVHRR instruments (*NOAA-7* through *NOAA-18*) and both MODIS instruments (*Terra* and *Aqua*) are given. Relative differences in inferred reflectance using the various irradiance datasets are also given for each instrument. We conclude with a discussion on the impact of solar irradiance uncertainty on cloud microphysical retrievals.

2. Overview of historical 3.7-μm spectral irradiance datasets

The only observational absolute spectral irradiance dataset covering the 3.7-μm band was obtained during the August 1967 aircraft campaign described by Thekaekara et al. (1969) and Thekaekara (1974). Instrument and analysis details of the flights off the coast of California are extensively discussed in Thekaekara et al. (1969) and summarized here.

Measurements were made from the NASA Convair CV-990 aircraft flying at an altitude of 11.5 km. During the six-flight campaign, a variety of total and spectral irradiance measurements were obtained from 12 instruments, only two of which measured spectral irradiance in the 3.7-μm band: a prism monochrometer (operated by Thekaekara et al.) and a Michaelson interferometer. To obtain irradiance over the entire solar disk, the monochrometer used a diffuse incident mirror with radiometric calibration traceable to a standard lamp; corrections were required to account for the additional optical path of sunlight through a sapphire window on the aircraft. The interferometer was calibrated to an onboard blackbody with corrections for detector and instrument emission. A "weighted average" of irradiance from the monochrometer and interferometer instruments was reported for the 3.7-μm band though no details on the weighting were given. An overall statement of the derived spectral irradiance accuracy was estimated at $\pm 5\%$. This assessment was not specified as a function of wavelength. Spectral irradiance in the 3.7-μm band was reported at 100-nm resolution. All irradiances were normalized to the average sun–Earth distance (1 AU).

Observations were made over a range of solar zenith angles and so corrections for slant path (air mass), as well as the atmospheric path absorption, are critical. In the visible portion of the spectrum, airmass corrections derived from the Langley plot method for a single flight day were used to extrapolate observations to zero air mass for all flights (with the implicit assumption that the above-flight level amount of absorbing gases and aerosol did not significantly change during the multiday observations). Otherwise, it appears that a zero airmass correction was obtained from a weighted average of solar zenith angle observations and ground-based airmass calculations (details on the weighting not described). Atmospheric spectral attenuation calculations are those of Elterman and Toolin (1965) for the U.S. Standard Atmosphere. Table 7-4 in Elterman and Toolin provides optical properties at 3.5 and 4.0 μm; at both wavelengths, the optical thickness between 11 km and TOA is given as zero. Molecular absorption in the 3.7-μm band is now known to be important (primarily CH_4 and N_2O in the short and longer wavelength portions of the band, respectively, along with water vapor absorption throughout the band). We performed our own calculations using the Moderate Spectral Resolution Atmospheric Transmittance (MODTRAN) atmospheric transmittance code (Berk et al. 2003) for a midlatitude summer standard atmosphere, an atmospheric path from 11 km to TOA, and an air mass of 2 (air masses over the course of the six CV-990 flights ranged from near unity to 7). Averaged over 50-nm bandpasses (estimated grating resolution at these wavelengths), the atmospheric path absorptance was 0.024, 0.006, 0.006, 0.040, and 0.021 at 3.6, 3.7, 3.8, 3.9, and 4.0 μm, respectively. Though a critical function of air mass, it appears that a significant 2%–4% absorption on either side of the 3.7-μm atmospheric window was likely even at CV-990 altitudes and not accounted for in the analysis.

Absolute radiance measurements in the spectral region include those of Kondratyev et al. (1965), obtained from Mt. Elbrus in the Caucasus Mountains (5.6-km altitude) over a 2-yr period, who reported results for the solar disk center at 3.0, 3.6, and 4.0 μm. Their results were converted to irradiance by Pierce and Allen (1977), along with the radiance measurements of Koutchmy and Peyturaux (1970) from Mt. Louis in the Pyrenees at 3.8 μm and the 31-km altitude balloon measurements of Murcray et al. (1964) at 4.0 and 4.1 μm. However, the solar limb darkening curve(s) used for the Pierce and Allen calculations was not discussed. The derived spectral irradiances for Kondratyev et al. are about 15% smaller than Thekaekara et al. at 3.6 μm; the Koutchmy and Peyturaux derived irradiance is identical with Thekaekara (at 1 W m^{-2} μm^{-1} precision); irradiances for Murcray et al. are 14% smaller than Thekaekara et al. at both wavelengths. Kondratyev et al. give uncertainties of a few percent in the 3.7-μm band, as does Murcray et al. for their 4–5-μm measurements. A summary of these and other historical solar spectral observations is given in Pierce and Allen (1977).

High spectral resolution interferometer observations of solar disk center radiance covering the midwave infrared have also been published. These data include the ATMOS space shuttle experiment Fourier transform spectrometer observations (Farmer 1994) and the ground-based Kitt Peak atlas of Livingston and Wallace (1991). However, these data were intended for spectroscopic studies and are not absolutely calibrated.

Several compilations of observational and/or modeled solar irradiance spectra are in wide use by the remote sensing community. The World Radiation Center (WRC) Reference Spectrum (Wehrli 1985) adopted by the World Meteorological Organization (WMO) is a compilation from a number of sources. For the present discussion, irradiance in the midwave infrared portion of the spectrum comes from Smith and Gottlieb (1974), which is in turn, a compilation of several sources. All data points from Smith and Gottlieb in the 3.7-μm spectral region are from the few Koutchmy and Peyturaux (1970) and Murcray et al. (1964) radiance measurements previously discussed; again, no information is given regarding the limb-darkening curves used for the radiance to irradiance conversion in this spectral region. To compensate for the sparse data in this spectral region, Smith and Gottlieb provided the coefficients of a linear fit to a log–log plot of the available data; this means interpolation is apparently used to provide the 10-nm resolution found in Wehrli.

A dataset by Kurucz (1995) was incorporated into the MODTRAN radiative transfer model along with some later modifications (Berk et al. 2003; see file DATA/newkur.dat in the MODTRAN4 distribution). While MODTRAN4 provides options for using other irradiance datasets for various parts of the solar spectrum, the Kurucz quiet-sun spectrum is the sole dataset covering the 3.7-μm spectral region. From the available documentation, the Kurucz spectrum is calculated using a quiet-sun solar atmospheric model and lines and atomic data compiled by Kurucz. The American Society for Testing and Materials (2000) E-490 solar spectrum, developed for use by the aerospace community, also uses the Kurucz spectra in the 3.7-μm band.

3. New spectral irradiance calculations

With only a single absolute observational irradiance dataset available, and difficulty and/or lack of information for deriving irradiance uncertainties from the solar radiance observations, it is important to include information available from solar models in assessing the state of the knowledge for this spectral region. Here we give a brief description of calculations using the Fontenla et al. (2006) published set of solar models that were further developed by Fontenla et al. (2007) and describe the relevant atomic and molecular data for computing the spectrum in the 3.7-μm band. We then compare our results with the historical datasets described in section 2. The newly computed quiet-sun spectrum from Fontenla et al. (2006) as implemented in the Solar Radiation Physical Modeling (SRPM) system (described below) and covering a spectral range from the UV to centimetric radio wavelengths, is planned for inclusion in the upcoming MODTRAN5 release (G. Anderson 2006, personal communication).

a. Overview of the model

The solar irradiance spectrum is calculated from the model atmospheres of solar surface features reported by Fontenla et al. (2006). Model C from that dataset is used in this study. The model consists of solar atmospheric parameters as a function of height that are based on earlier work and constrained by comparisons with available ground and space observations of line profiles and continuum of the emitted radiance at visible and infrared wavelengths. Among these observations, absolutely calibrated space-based observations of the solar spectral irradiance in the visible and near IR, especially those from the solar spectrum spectrometer (SOLSPEC; Thuillier et al. 2003), provide an absolute

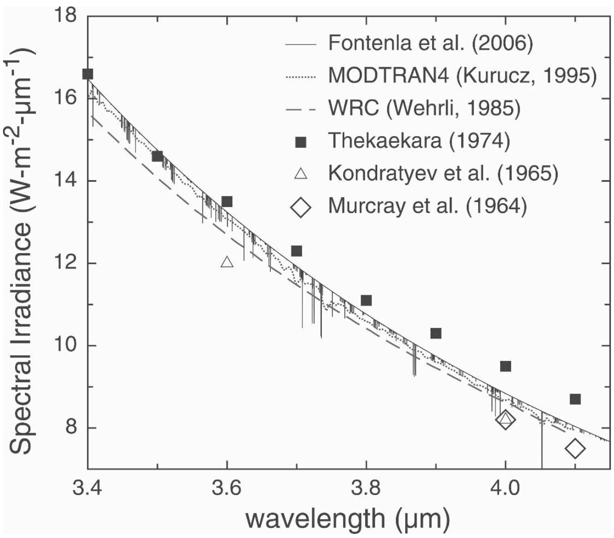

FIG. 1. Plot of selected solar spectral irradiance datasets discussed in the text for the 3.7-μm band spectral region. Data points for Kondratyev et al. and Murcray et al. were taken from Pierce and Allen (1977).

temperature scale. Because these absolutely calibrated observations used for the models were obtained at shorter wavelengths (e.g., maximum wavelength from Thuillier et al. is 2.4 μm), the computed spectral irradiance in the 3.7-μm band relies on the physical model of the solar atmosphere derived from those observations and knowledge of absorption and emission radiative coefficients in the solar atmosphere.

The emergent irradiance spectrum from model C is computed at 1 AU in the manner described by Fontenla et al. (1999, 2006; as implemented in the Solar Radiation Physical Modeling system). The SRPM calculations show that the 3.7-μm continuum irradiance originates in photospheric layers with gas pressures between 0.57×10^5 and 1.08×10^5 dyne cm^{-2} (heights from about 10 to 100 km above the $\tau_{500\mathrm{nm}} = 1$ level, and temperatures in the range 5480 to 6310 K), and these layers encompass the significant formation of emitted radiance at all positions on the solar disk. The irradiance spectrum at 3.7 μm consists of a predominant continuum with a number of weak CO and OH molecular lines (only a few that are significant). Atomic lines of O, N, S, and C are also present but are not significant for the broadband calculations discussed in later sections. The lines we compute are evident in Fig. 1 at subangstrom resolution, but because of a lack of reliable atomic data our calculated spectrum may contain a few less lines than the actual solar spectrum. However, the overall effects of the lines are small and only at longer wavelengths (about 4.295 μm, outside the band we consider) do CO bands become strong enough to produce a significant reduction in the broadband irradiance.

The main atomic parameter in the 3.7-μm band is the free–free opacity of the negative ion of hydrogen. Fontenla et al. (2007) updated older estimates used in Fontenla et al. (2006) to the values published by Bell and Berrington (1987) and this produced some changes to the infrared intensities computed by SRPM. These opacity values are now thought to be accurate to within 2% (John 1988), which, taking into account the temperature gradient in the region of continuum formation, would result in about a 0.5% irradiance error.

However, the SRPM computed irradiance spectrum is 2.2% below Thuillier et al. (2003) at their longest measured wavelength (2.40 μm). This suggests that the 3.7-μm irradiance may be similarly underestimated in our calculations by perhaps 2%. Such an error is higher than what is estimated from the atomic data uncertainty but well within the combined error of the atomic data plus observations (~2% according to Thuillier et al. 2003).

The Fontenla et al. (2006) models considered irradiance changes related to the solar activity cycle and rotation. Using the methods described by Fontenla and Harder (2005), it was found that the variations in solar irradiance in the 3.7-μm spectral region due to solar activity were less than ~0.5% of the quiet-sun irradiance during the last 2 yr. The magnitude of these variations are confirmed by the variability observed at visible and shorter IR wavelengths by the Spectral Irradiance Monitor (SIM) on board the Solar Radiation and Climate Experiment (SORCE) satellite (Harder et al. 2005; Rottman et al. 2005). The layers producing the 3.7-μm irradiance are just a bit shallower than those producing the visible irradiance at the continuum around 800 nm, and the observed and modeled irradiance variations are close to what is observed at that wavelength. Consequently, the model estimated variability at 3.7 μm is believed to be close to the real variability. These irradiance variations are relatively small when compared with an uncertainty of about 2% in the overall value, which, as explained above, is due to combined uncertainties in the available spectral irradiance observations and atomic data.

b. *Model spectrum and comparisons with other datasets*

Spectral irradiance from Fontenla et al. (2006) is plotted in Fig. 1. Line features are evident, especially around 4.05 μm, though they are relatively insignificant when compared with continuum emission. All subsequent calculations use a reduced resolution form of the high-spectral-resolution model output shown in the figure (convolution of the high-resolution data with a 1-nm FWHM filter).

The irradiance curve of Fig. 1 is well approximated over the spectral range 3.40–4.15 μm (mean absolute deviation of 0.029 W m^{-2} μm^{-1} or about 0.3% relative) by the following quadratic function:

$$F_0(\lambda) = 157.91 - 66.34\lambda + 7.265\lambda^2, \quad (4)$$

with λ in micrometers and $F_0(\lambda)$ in watts per meter squared per micrometer. Writing Eq. (4) in terms of wavenumber gives

$$F_0(\nu) = \frac{157.91 \times 10^4}{\nu^2} - \frac{66.34 \times 10^8}{\nu^3} + \frac{7.265 \times 10^{12}}{\nu^4}, \quad (5)$$

with ν in inverse centimeters and $F_0(\nu)$ in watts per meter squared per inverse centimeter. As discussed in the next section, these analytic fits give band-averaged irradiances to about the 0.1% level or better relative to the actual Fontenla et al. spectrum. Brightness temperature is approximately linear across the spectral range (plot not shown) and can be accurately fit (4.3-K mean absolute deviation over the range 3.40–4.15 μm) by

$$T_B(\lambda) = 6533.6 - 229.6\lambda, \quad (6)$$

with λ in micrometers and T_B in kelvin.

Plots of the datasets discussed in section 2 are also shown in Fig. 1. As a reminder, other than the Kurucz (1995) spectrum, these historical data are observational, though all except Thekaekara (1974) are derived from disk center radiance measurements. The Thekaekara irradiance is uniformly larger than all other datasets except at the shorter wavelengths where values are roughly the same as the Fontenla et al. (2006) and Kurucz spectrum. The Fontenla et al. and Kurucz spectra generally give irradiances within a couple of percent of each other, though the latter model shows more significant line features in the center of the 3.7-μm band. There is insufficient documentation on the Kurucz (1995) solar model and atomic and molecular data sources to compare with those used in our calculations. The Wehrli (1985) spectrum is positively biased relative to the Kondratyev et al. (1965) and Murcray et al. (1964) data points, despite the fact that these data were the ultimate source for the Smith and Gottlieb (1974) fits adopted by Wehrli; however, as noted in the section 2, the limb-darkening curve used by Smith and Gotlieb to convert these data to irradiance is not likely the same as the curve used by Pierce and Allen (1977), whose tabular values are shown in Fig. 1.

c. Instrument-specific sensitivity to the irradiance spectrum

Uncertainty in inferring the bidirectional reflectance from a 3.7-μm channel observation is dependent on the uncertainty in the instrument spectral response function, the solar irradiance spectrum, and the instrument's radiance calibration uncertainty [Eq. (1)].

The relative spectral response functions for the 3.7-μm channel for four of the 10 AVHRR instruments considered in this study, and the two MODIS instruments, are shown in Fig. 2. The Fontenla and Thekaekara spectral irradiance data (from Fig. 1) are also shown. The calculated bandpass and central wavelength in micrometers for both MODIS and all 10 AVHRR instruments is given in Table 1. The two MODIS response functions are very similar while there is wide variation in the AVHRR channel characteristics (differences in central wavelength of over 90 nm between *NOAA-12* and *NOAA-15*). All response functions are based on prelaunch measurements. *NOAA-16* flew the first AVHRR instrument characterized using a new automated spectral response function system with high spectral resolution capability. It was discovered that there had been a problem with the *NOAA-16* AVHRR measurement setup after the satellite had been launched. Since an end-to-end spectral response measurement was no longer possible, a piecewise response function was calculated from each optical path component. This piecewise calculation is currently preferred over the original measurement (J. Sullivan, NOAA/NESDIS, 2006, personal communication).

While AVHRR and MODIS instruments are filter radiometers, MODIS interference filters are made with a more stable ion-assisted deposition process (Montgomery et al. 2000). Further, MODIS has an onboard calibration source to monitor in-orbit changes in the channel center for spectral channels from the visible up to 2.1 μm (the Spectral Radiometric Calibration Assembly; Montgomery et al. 2000) and no significant spectral shifts have been observed in these channels for either MODIS instrument (e.g., less than 0.2 nm for shortwave infrared channels; Xiong et al. 2005a). While 3.7-μm spectral stability cannot be monitored in orbit, performance similar to the shorter wavelength channels is expected.

The differences in filter location and bandpass seen in Fig. 2 result in substantial differences in the calculated average solar spectral irradiance over the channel [Eq. (2)]; such calculations for each instrument are given in Tables 2 and 3 for the Fontenla et al. (2006), Thekaekara (1974), and Kurucz (1995) spectra. In the

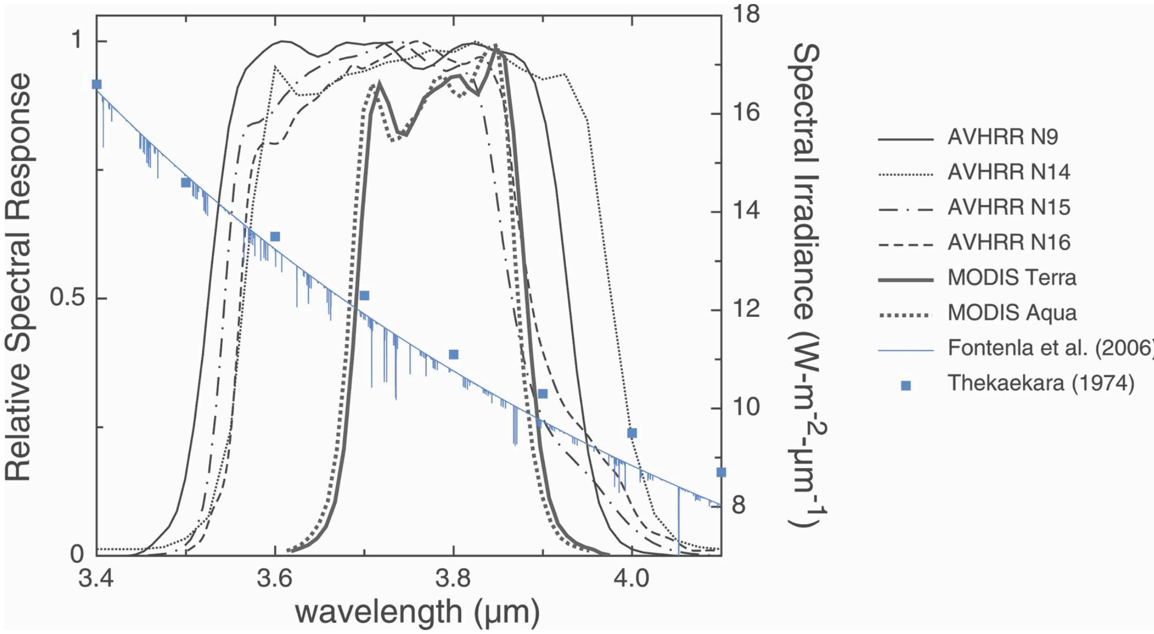

FIG. 2. The 3.7-μm channel relative spectral response functions for the two MODIS instruments (NASA *Terra* and *Aqua* spacecrafts) and a subset of the AVHRR instruments (NOAA polar orbiting platforms *9*, *14*, *15*, and *16*) used for channel-averaged irradiance calculations. The solar spectral irradiance from Fontenla et al. (2006) and Thekaekara (1974), taken from Fig. 1, is also shown.

calculations, we integrated between the 0.02 relative spectral response function points. No attempt was made to account for low-level out-of-band responses. This includes the purported 4.2-μm spectral leak into the 3.7-μm channel of AVHRR *NOAA-16* (A. Heidinger, NOAA/NESDIS, 2006, personal communication); this leak is unlikely to have any significant impact because of the earth's atmospheric CO_2 absorption. Regardless, out-of-band responses would in practice be handled best separately in radiative transfer calculations because of spectrally varying cloud and surface properties. The differences in channel-averaged irradiances from Table 2 relative to the Fontenla spectrum are given by the first pair of data columns in Table 4. As an example, for the MODIS *Terra* response function, use of the Thekaekara data results in an averaged spectral irradiance 3.85% larger than that obtained from Fontenla and 5.45% larger than use of the Kurucz

TABLE 1. The spectral response function full-width-at-half-maximum (FWHM) bandpass and central wavelength (defined as the average of the two FWHM wavelengths) for AVHRR and MODIS 3.7-μm channels used in this study.

Instrument/platform	Central wavelength (μm)	Bandpass (μm)
AVHRR N7	3.741	0.411
AVHRR N9	3.733	0.410
AVHRR N10	3.763	0.375
AVHRR N11	3.750	0.400
AVHRR N12	3.800	0.400
AVHRR N14	3.788	0.425
AVHRR N15	3.708	0.322
AVHRR N16	3.724	0.326
AVHRR N17	3.761	0.385
AVHRR N18	3.768	0.385
MODIS *Terra*	3.792	0.190
MODIS *Aqua*	3.785	0.189

TABLE 2. Channel-averaged solar spectral irradiance for AVHRR and MODIS 3.7-μm instrument channels for three spectral irradiance datasets.

	Band-averaged solar spectral irradiance (W m^{-2} μm^{-1})		
	Solar irradiance dataset		
Instrument/platform	Fontenla et al. (2006)	Thekaekara (1974)	Kurucz (1995)
AVHRR N7	11.573	11.957	11.429
AVHRR N9	11.671	12.043	11.528
AVHRR N10	11.360	11.771	11.216
AVHRR N11	11.543	11.930	11.400
AVHRR N12	11.020	11.470	10.879
AVHRR N14	11.138	11.573	10.997
AVHRR N15	11.729	12.101	11.577
AVHRR N16	11.467	11.867	11.317
AVHRR N17	11.327	11.741	11.184
AVHRR N18	11.200	11.627	11.059
MODIS *Terra*	10.885	11.304	10.720
MODIS *Aqua*	10.974	11.386	10.807

TABLE 3. As in Table 2 but in wavenumber spectral density.

Instrument/platform	Band-averaged solar spectral irradiance ($W/m^2\ cm^{-1}$)x100 — Solar irradiance dataset: Fontenla et al. (2006)	Thekaekara (1974)	Kurucz (1995)
AVHRR N7	1.6096	1.6644	1.5895
AVHRR N9	1.6159	1.6710	1.5970
AVHRR N10	1.5890	1.6442	1.5681
AVHRR N11	1.6060	1.6586	1.5850
AVHRR N12	1.5655	1.6261	1.5454
AVHRR N14	1.5757	1.6335	1.5550
AVHRR N15	1.6189	1.6777	1.5963
AVHRR N16	1.6019	1.6606	1.5819
AVHRR N17	1.5929	1.6481	1.5724
AVHRR N18	1.5842	1.6395	1.5650
MODIS *Terra*	1.5607	1.5739	1.5384
MODIS *Aqua*	1.5666	1.5810	1.5432

spectrum. Similar values are found in the second pair of columns in Table 4 where the irradiance differences have been given in terms of solar reflectance [Eqs. (1) and (2)]. Note that the difference in the average irradiance between the two MODIS instruments is less than 0.5%, regardless of the irradiance spectrum used, while AVHRR differences can be in excess of 6% (*NOAA-12* versus *NOAA-15*).

For context, the calibration of MODIS solar bands used for cloud retrieval algorithms (visible through the 2.1-μm band) is derived from an onboard solar diffuser; including transfer of the diffuser calibration to the onboard diffuser observation, uncertainty is less than 2% for most solar bands (Xiong et al. 2005b). Instrument-specific uncertainties related to the 3.7-μm characterization of onboard blackbody calibration sources and their transfer need to be added appropriately to the numbers in Table 4 (e.g., addition of variances assuming zero correlation) to provide an overall reflectance measurement uncertainty. The total RMS onboard radiance calibration uncertainty for the MODIS 3.7-μm channel (referred to as band number 20) has been evaluated to be less than 0.7% over a wide range of radiances for both *Terra* and *Aqua* instruments (Xiong et al. 2005b). Therefore, for MODIS, the solar irradiance uncertainties of Table 4 dominate the radiometric and spectral uncertainties and thus also dominate the reflectance calculation uncertainty. Issues related to AVHRR thermal channel radiometric uncertainty and stability are discussed by Trishchenko (2002) and Trishchenko et al. (2002).

We used the analytic fits derived in the last section [Eqs. (4) and (5)] as a substitute for the Fontenla et al. (2006) irradiance spectrum and recalculated the band-averaged irradiances in Tables 2 and 3. For the 12 AVHRR and MODIS instruments in those tables, the band-averaged solar irradiance derived from Eqs. (4) and (5) was not more than 0.1% different than those derived directly from the Fontenla et al. spectrum, with the exception of the *NOAA-15* AVHRR, which showed a 0.12% difference. For the MODIS instruments, the differences were better than 0.01%. Thus the equations provide band-averaged irradiances to a precision that is about a factor of 20 (or more) better than the estimated accuracy of the Fontenla et al. spectrum in this region (2% relative) and similarly smaller than the differences between the irradiance datasets compared in Table 4. As such, Eqs. (4) and (5) can be used for typical spectroradiometer 3.7-μm bandpass

TABLE 4. Difference in the 3.7-μm channel-averaged solar spectral irradiance and inferred solar reflectance relative to the Fontenla et al. (2006) dataset, as derived from Table 2.

Instrument/platform	Relative difference (%) in solar irradiance vs Fontenla irradiance dataset		Relative difference (%) in inferred solar reflectance vs Fontenla irradiance dataset	
	Thekaekara (1974)	Kurucz (1995)	Thekaekara (1974)	Kurucz (1995)
AVHRR N7	3.32	−1.24	−3.21	1.26
AVHRR N9	3.19	−1.23	−3.09	1.24
AVHRR N10	3.62	−1.27	−3.49	1.28
AVHRR N11	3.35	−1.24	−3.24	1.25
AVHRR N12	4.08	−1.28	−3.92	1.30
AVHRR N14	3.91	−1.27	−3.76	1.28
AVHRR N15	3.17	−1.30	−3.07	1.31
AVHRR N16	3.49	−1.31	−3.37	1.33
AVHRR N17	3.65	−1.26	−3.53	1.28
AVHRR N18	3.81	−1.26	−3.67	1.27
MODIS *Terra*	3.85	−1.52	−3.71	1.54
MODIS *Aqua*	3.75	−1.52	−3.62	1.55

calculations without incurring any significant error in retrievals (see next section for cloud retrieval error context); exceptions would include narrowband spectrometers in the CO line portion of the solar atmosphere spectrum (Fig. 1).

d. *Cloud retrieval sensitivity*

The significance of the reflectance differences in Table 4 for cloud retrieval applications was empirically investigated using a *Terra* MODIS data granule of coastal Chile and Peru that has been previously discussed (Platnick et al. 2003). The granule (5 min of data) includes a variety of cloud types, including marine boundary layer water clouds, cirrus over land and ocean, and convective ice and water clouds over the Amazon basin. Retrievals were obtained from the operational MODIS *Terra* cloud product (MOD06) collection 5 processing stream code, which includes separate effective retrievals derived from 3.7-μm MODIS observations (as well as size retrievals derived from 1.6 and 2.1 μm observations, separately and in combination). Histograms of liquid water and ice cloud effective radius retrievals for the data granule are shown in Fig. 3 using two different values for the 3.7-μm MODIS channel-averaged spectral irradiance (a 5% difference). The 11.34 W m^{-2} μm^{-1} value corresponds to the average of the MODIS *Terra* and *Aqua* instrument irradiances using the Thekaekara (1974) dataset. The smaller irradiance (10.77 W m^{-2} μm^{-1}) is comparable to the instrument averages using either Fontenla et al. (2006) or Kurucz (1995). For liquid water clouds, the difference in the mean value of the retrieved effective radius over the data granule is 0.50 μm ($\approx$4.5%); for ice clouds, the difference is 0.71 μm ($\approx$6.5%).

To place these differences in context, the 3.7-μm effective radius retrieval uncertainty for these MODIS retrievals was calculated assuming the spectral irradiance is known exactly but including the following set of error sources contributing to the reflected signal: instrument calibration and forward model uncertainty (5%), surface spectral albedo uncertainty (15%), and above-cloud column water vapor amount derived from model analysis and MODIS cloud-top pressure retrievals for use in spectral atmospheric corrections (20%). Each error source is assumed uncorrelated. Note that the uncertainty analysis does not include errors in the estimation of cloud-top temperature, surface temperature, and atmospheric state that are required to account for the 3.7-μm emission component. The retrieval uncertainty is a function of effective radius and cloud optical thickness, as well as surface type and atmospheric state and as such is difficult to summarize succinctly (Platnick et al. 2004). However, for comparison with the granule-averaged means of Fig. 3, mean 3.7-μm effective radius relative uncertainties are 5.2% and 6.4% for liquid water and ice clouds, respectively. Therefore, in this example, the uncertainty in the retrieved effective radius due to a 5% irradiance uncertainty is of the same order as other fundamental reflectance error sources.

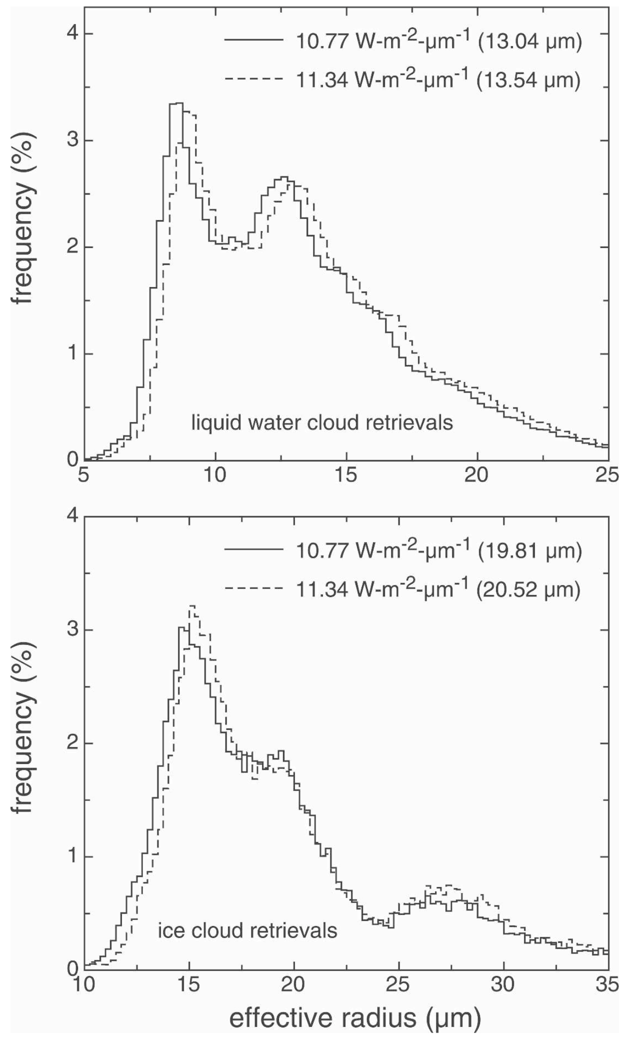

FIG. 3. Frequency histogram for (top) liquid water and (bottom) ice cloud retrievals from a MODIS *Terra* data granule (see text for details) using two different values for the channel-averaged spectral irradiance. The mean effective radius for the retrievals is given in parentheses.

4. Discussion

Despite the widespread presence of a 3.7-μm atmospheric window channel on present-day and planned satellite imagers, the absolute top-of-atmosphere solar spectral irradiance in the band, which is required for daytime quantitative use, is limited to a single aircraft field campaign (Thekaekara et al. 1969; Thekaekara 1974). This sole observational irradiance dataset was discussed, along with a survey of published radiance observations, and compared with historical synthetic datasets and the new solar models of Fontenla et al. (2006, 2007). Channel-averaged spectral irradiances using the various datasets were calculated for laboratory-derived AVHRR and MODIS instrument spectral response functions. Depending on the particular instrument, the observations reported by Thekaekara (1974) give averaged irradiances from about +3.2% to +4.1% greater than the quiet-sun Fontenla et al. (2006) spectrum; the Kurucz spectra give channel-averaged irradiances about −1.2% to −1.5% smaller than Fontenla et al. The new Fontenla et al. irradiance spectrum is expected to have a 2% uncertainty in the 3.7-μm region.

The consequences on cloud microphysical retrievals from uncertainty in the 3.7-μm band solar irradiance was examined for a MODIS data granule consisting of a variety of liquid and ice clouds over both ocean and land. Using a representative channel-averaged solar irradiance uncertainty of 5%, based on this study's comparisons of observational and modeled irradiances, averaged retrieved effective radius uncertainties averaged for all pixels in the data granule were 4.5% and 6.5% for liquid water and ice clouds, respectively. This is comparable to retrieval uncertainties due to other error sources that fundamentally impact the inference of cloud-top reflectance in the band. Retrieval uncertainties from errors in estimating emitted radiance in the channels were not considered.

The quiet-sun irradiance spectrum from Fontenla et al. used in this study [as implemented in the Solar Radiation Physical Modeling (SRPM) system] is planned for inclusion in the upcoming MODTRAN5 release. In the meantime, analytic fits to the Fontenla et al. spectral irradiance and brightness temperature from 3.4 to 4.15 μm have been provided [Eqs. (4)–(6)]. For the AVHRR and MODIS instruments of Tables 2 and 3, the irradiance fits provide band-averaged irradiance precision in the 3.7-μm channels to about the 0.1% level or better.

While the relative agreement between modeled spectra and Thekaekara (1974) in the 3.7-um band is reassuring, new absolute spectral irradiance observations in the band are sorely needed to augment the sole available observations reported by Thekaekara.

Acknowledgments. This research was supported in part by the NASA Radiation Science Program under Grant 621-30-92 (SP); JMF was supported by Contract NAS5-97045 at the University of Colorado. We are grateful to Drs. Andrew Heidinger at NOAA/NESDIS and Xiaoxiong ("Jack") Xiong at the NASA Goddard Space Flight Center for their input and to anonymous reviewers for helpful comments and suggestions.

REFERENCES

Ackerman, S. A., K. I. Strabala, W. P. Menzel, R. A. Frey, C. C. Moeller, and L. E. Gumley, 1998: Discriminating clear-sky from clouds with MODIS. *J. Geophys. Res.,* **103,** 32 141–32 158.

American Society for Testing and Materials, cited 2000: Standard extraterrestrial spectrum reference E-490. [Available online at http://www.astm.org.]

Aminou, D. M. A., 2002: MSG's SEVIRI instrument. *Eur. Space Agency Bull.,* **111,** 15–17.

Arking, A., and J. D. Childs, 1985: Retrieval of cloud cover parameters from mutispectral satellite images. *J. Climate Appl. Meteor.,* **24,** 322–333.

Barnes, R. A., W. L. Barnes, C.-H. Lyu, and J. M. Gales, 2000: An overview of the visible and infrared scanner radiometric calibration algorithm. *J. Atmos. Oceanic Technol.,* **17,** 395–405.

Barnes, W. L., T. S. Pagano, and V. V. Salomonson, 1998: Prelaunch characteristics of the Moderate Resolution Imaging Spectroradiometer (MODIS) on EOS-AM1. *IEEE Trans. Geosci. Remote Sens.,* **30,** 2–27.

Bell, K. L., and K. A. Berrington, 1987: Free-free absorption coefficient of the negative hydrogen ion. *J. Phys. B,* **20,** 801–806.

Berk, A., and Coauthors, 2003: *MODTRAN4 Version 3 Revision 1 User's Manual.* Air Force Research Laboratory, 91 pp.

Elterman, L., and R. B. Toolin, 1965: *Handbook of Geophysics and Space Environments,* S. L. Valley, Ed., McGraw-Hill.

Farmer, C. B., 1994: The ATMOS solar atlas. *Infrared Solar Physics: Proceedings of the 154th Symposium of the International Astronomical Union,* D. M. Rabin, J. T. Jefferies, and C. Lindsey, Eds., Kluwer Academic, 511–521.

Fontenla, J. M., and J. W. Harder, 2005: Physical modeling of spectral irradiance variations. *Mem. Soc. Astron. Ital.,* **76,** 826–833.

——, O. R. White, P. A. Fox, E. H. Avrett, and R. L. Kurucz, 1999: Calculation of solar irradiances. I. Synthesis of the solar spectrum. *Astrophys. J.,* **518,** 480–499.

——, E. Avrett, G. Thuillier, and J. Harder, 2006: Semiempirical models of the solar atmosphere. I. The quiet- and active sun photosphere at moderate resolution. *Astrophys. J.,* **639,** 441–458.

——, K. S. Balasubramaniam, and J. Harder, 2007: Semiempirical models of the solar atmosphere. II. The quiet-sun low chromosphere at moderate resolution. *Astrophys. J.,* **667,** 1243–1257.

Han, Q., W. B. Rossow, and A. A. Lacis, 1994: Near-global survey of effective droplet radii in liquid water clouds using ISCCP data. *J. Climate,* **7,** 465–497.

Harder, J. W., J. M. Fontenla, O. White, G. Rottman, and T. Woods, 2005: Solar spectral irradiance variability comparisons of the SORCE SIM instrument with monitors of solar activity and spectral synthesis. *Mem. Soc. Astron. Ital.,* **76,** 735–742.

Heidinger, A. K., V. Rao, A. Dean, and C. Dean, 2002: Using MODIS to estimate cloud contamination of the AVHRR data record. *J. Atmos. Oceanic Technol.,* **19,** 586–601.

John, T. L., 1988: Continuous absorption by the negative hydrogen ion reconsidered. *Astron. Astrophys.,* **193,** 189–192.

Justice, C. O., and Coauthors, 2002: The MODIS fire products. *Remote Sens. Environ.,* **83,** 244–262.

Kaufman, Y. J., C. J. Tucker, and I. Fung, 1990: Remote sensing of biomass burning in the tropics. *J. Geophys. Res.,* **95,** 9927–9939.

King, M. D., and Coauthors, 1996: Airborne scanning spectrometer for remote sensing of cloud, aerosol, water vapor, and surface properties. *J. Atmos. Oceanic Technol.,* **13,** 777–794.

Kondratyev, K. Y., S. D. Andreev, I. Y. Badinov, V. S. Grishechkin, and L. V. Popova, 1965: Atmospheric optics investigations on Mt. Elbrus. *Appl. Opt.,* **4,** 1069–1076.

Koutchmy, S., and R. Peyturaux, 1970: Study of the solar continuum in the intermediate infra-red spectral range 3.5-24.4 μ. *Astron. Astrophys.,* **5,** 470–487.

Kurucz, R. L., 1995: The solar irradiance by computation. *Proceedings of the 17th Annual Review Conference on Atmospheric Transmission Models,* G. P. Anderson, R. H. Picard, and J. H. Chetwynd, Eds., PL/-TR-95-2060, Special Rep. 274, Pl. 332, Phillips Laboratory Geophysics Directorate.

Lee, T. E., S. D. Miller, F. J. Turk, C. Schueler, R. Julian, S. Deyo, P. Dills, and S. Wang, 2006: The NPOESS VIIRS day/night visible sensor. *Bull. Amer. Meteor. Soc.,* **87,** 191–199.

Livingston, W., and L. Wallace, 1991: An atlas of the solar spectrum in the infrared from 1.1 to 5.4 μm. National Solar Observatory Tech. Rep. 91-001.

Montgomery, H., N. Che, K. Parker, and J. Bower, 2000: The algorithm for MODIS wavelength on-orbit calibration using the SRCA. *IEEE Trans. Geosci. Remote Sens.,* **38,** 877–884.

Minnis, P., and Coauthors, 1995: Cloud optical property retrieval (subsystem 4.3). Clouds and the Earth's Radiant Energy System (CERES) Algorithm Theoretical Basis Document, Volume III: Cloud Analyses and Radiance Inversions (subsystem 4), CERES Science Team, Eds., NASA Rep. 1376, Vol. 3, 135–176.

Murcray, F. H., D. G. Murcray, and W. J. Williams, 1964: The spectral radiance of the sun from 4 micrometer to 5 micrometer. *Appl. Opt.,* **3,** 1373–1377.

Nakajima, T. Y., T. Nakajima, M. Nakajima, H. Fukushima, M. Kuji, A. Uchiyama, and M. Kishino, 1998: Optimization of the *Advanced Earth Observing Satellite II* Global Imager channels by use of radiative transfer calculations. *Appl. Opt.,* **37,** 3149–3163.

Pavolonis, M. J., A. K. Heidinger, and T. Uttal, 2005: Daytime global cloud typing from AVHRR and VIIRS: Algorithm description, validation, and comparisons. *J. Appl. Meteor.,* **44,** 804–826.

Pierce, A. K., and R. G. Allen, 1977: The solar spectrum between 3 and 10 μm. *The Solar Output and its Variation,* O. R. White, Ed., Colorado Associated University Press, 169–192.

Platnick, S., and S. Twomey, 1994: Determining the susceptibility of cloud albedo to changes in droplet concentrations with the Advanced Very High Resolution Radiometer. *J. Appl. Meteor.,* **33,** 334–347.

——, M. D. King, S. A. Ackerman, W. P. Menzel, B. A. Baum, J. C. Riédi, and R. A. Frey, 2003: The MODIS cloud products: Algorithms and examples from *Terra. IEEE Trans. Geosci. Remote Sens.,* **41,** 459–473.

——, R. Pincus, B. Wind, M. D. King, M. A. Gray, and P. Hubanks, 2004: An initial analysis of the pixel-level uncertainties in global MODIS cloud optical thickness and effective particle size retrievals. *Passive Optical Remote Sensing of the Atmosphere and Clouds IV,* S. C. Tsay, T. Yokota, and M.-H. Ahn, Eds., International Society for Optical Engineering (SPIE Proceedings Vol. 5652), 30–40.

Prins, E. M., and W. P. Menzel, 1992: Geostationary satellite detection of biomass burning in South America. *Int. J. Remote Sens.,* **13,** 2783–2799.

Rottman, G., J. Harder, J. Fontenla, T. Woods, O. R. White, and G. M. Lawrence, 2005: The spectral irradiance monitor (SIM): Early observations. *Sol. Phys.,* **230,** 205–244.

Saunders, R. W., and K. T. Kriebel, 1988: An improved method for detecting clear sky and cloudy radiances from AVHRR data. *Int. J. Remote Sens.,* **9,** 123–150.

Schmit, T. J., M. M. Gunshor, W. Paul Menzel, J. Li, S. Bachmeier, and J. J. Gurka, 2005: Introducing the next-generation Advanced Baseline Imager (ABI) on GOES-R. *Bull. Amer. Meteor. Soc.,* **86,** 1079–1096.

Schwalb, A., 1978: The TIROS-N/NOAA A-G satellite series. NOAA Tech. Memo. NESS 95, 75 pp.

Scorer, R. S., 1986: *Cloud Investigation by Satellite*. Halsted Press, 300 pp.

——, 1989: Cloud reflectance in channel-3. *Int. J. Remote Sens.,* **10,** 675–686.

Smith, E. V. P., and D. M. Gottlieb, 1974: Solar flux and its variation. *Space Sci. Rev.,* **16,** 771–802.

Thekaekara, M. P., 1974: Extraterrestrial solar spectrum, 3000-6100 Å at 1-Å intervals. *Appl. Opt.,* **13,** 518–522.

——, R. Kruger, and C. H. Duncan, 1969: Solar irradiance measurements from a research aircraft. *Appl. Opt.,* **8,** 1713–1732.

Thuillier, G., M. Hersé, D. Labs, T. Foujols, W. Peetermans, D. Gillotay, P. C. Simon, and H. Mandel, 2003: The solar spectral irradiance from 200 to 2400 nm as measured by the SOLSPEC spectrometer from the Atlas and Eureca missions. *Sol. Phys.,* **214,** 1–22.

Trishchenko, A. P., 2002: Removing unwanted fluctuations in the AVHRR thermal calibration data using robust techniques. *J. Atmos. Oceanic Technol.,* **19,** 1939–1954.

——, 2006: Solar irradiance and effective brightness temperature for SWIR channels of AVHRR/NOAA and GOES imagers. *J. Atmos. Oceanic Technol.,* **23,** 198–210.

——, G. Fedosejevs, Z. Li, and J. Cihlar, 2002: Trends and uncertainties in thermal calibration of AVHRR radiometers onboard NOAA-9 to NOAA-16. *J. Geophys. Res.,* **107,** 4778, doi:10.1029/2002JD002353.

Wehrli, C., 1985: Extraterrestrial solar spectrum. Physikalisch-Meteorologisches Observatorium Davos and World Radiation Center, Publication 615. [Available online at ftp://ftp.pmodwrc.ch/pub/data/irradiance/spectral_irradiance/wrc_spectrum.asc.]

Xiong, X., N. Che, B. Guenther, W. L. Barnes, and V. V. Salomonson, 2005a: Five years of *Terra* MODIS on-orbit spectral characterization. *Earth Observing Systems X,* J. J. Butler, Ed., International Society for Optical Engineering (SPIE Proceedings Vol. 5882), doi:10.1117/12.614090.

——, J. Sun, A. Wu, K.-F. Chiang, J. Esposito, and W. Barnes, 2005b: *Terra* and *Aqua* MODIS calibration algorithms and uncertainty analysis. *Sensors, Systems, and Next-Generation Satellites IX,* R. Meynart, S. P. Neeck, and H. Shimoda, Eds., International Society for Optical Engineering (SPIE Proceedings Vol. 5978), doi:10.1117/12.627631.